CLM - P 564

CLM - P 564

UKAEA

Preprint

MELTING FRONT PHENOMENA - ANALYSIS AND COMPUTATION

B D TURLAND
R S PECKOVER

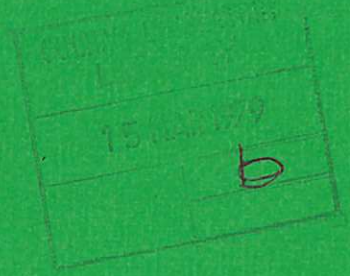

CULHAM LABORATORY
Abingdon Oxfordshire

1978

CLM-P564

MELTING FRONT PHENOMENA - ANALYSIS AND COMPUTATION

B D Turland and R S Peckover

UKAEA, Culham Laboratory, Abingdon, Oxon. OX14 3DB, UK

ABSTRACT

The rate and extent of melting front advance are important parameters both in the melt-through of reactor internals during the course of a hypothetical fission reactor meltdown accident and in the growth of a meltpool within an ex-vessel sacrificial bed if fitted as an additional core debris containment barrier

The time for a steel plate to melt through for a given loading of core debris determines the integrity of dish type core catchers and delay times resulting from core support structures. An accurate and economical numerical method for carrying out this calculation is presented.

The volume of a meltpool in a sacrificial bed can usefully be examined to a first approximation by assuming the pool grows radially using a mean heat transfer coefficient from the turbulently convecting molten pool. Based on appropriate approximate temperature profiles in the bed, pool growth can be well described by a single ordinary differential equation, and the maximum size expressed by simple formulae.

Results of sensitivity studies for pool growth using the PAMPUR 3 code, in which it is assumed that the pool shape is hemispheroidal, are reported.

The isotherm migration method for solving numerically the coupled melting and heat diffusion problem, which is used in a quasi-1D form in PAMPUR 3, has been generalised to handle multi-dimensional problems in a conservative formulation.

(Paper presented at Fourth Post Accident Heat Removal Conference, Ispra Joint Research Centre, 10th - 13th October 1978).

November 1978

MELTING FRONT PHENOMENA - ANALYSIS AND COMPUTATION

B D TURLAND AND R S PECKOVER

UKAEA Culham Laboratory, Abingdon, Oxon, U.K.

1. INTRODUCTION

The rate and extent of melting front advance are important parameters both in the melting of reactor internals during the course of a hypothetical reactor meltdown accident and in the growth of a meltpool within an ex-vessel sacrificial bed, if it were to be fitted as an additional core debris containment barrier.

Results of earlier investigations of ours were presented in [1]. This paper is a continuation of the approach described there, and consists of four parts. In the first, an accurate and economical method of calculating the melting attack on a plane slab is discussed. Second, approximate methods are given for tracking the position of the melting front and calculating the maximum size reached by a hemispherical melt pool, based on assumed temperature profiles in the bed material. Third, the sensitivity of pool growth to the values of some thermophysical properties is examined using the PAMPUR code. Finally, the formulation of the isotherm migration method (IMM) in conservative multidimensional form is outlined.

2. PLANE GEOMETRY: AN ECONOMICAL FINITE DIFFERENCE METHOD

The attack of heat producing core debris on horizontal steel surfaces such as a flat tray core catcher, internal support structure and the bottom of the reactor vessel may be largely one-dimensional. Efficient and accurate algorithms have been developed to model the advance of a plane melting front into a slab, incorporating heat diffusion within the slab and heat transfer to a sink. Fox [2] has summarised a number of schemes that have been proposed and tested for similar problems, but most of these have only been implemented in explicit form. The present calculations use the efficient implicit Crank-Nicolson method [3] to solve the diffusion equation within the slab, combined with second order accurate treatment of the boundary conditions. The calculational domain changes as the slab melts and so if, as is most suitable, a constant mesh interval is retained, there is a non-integer number of mesh intervals in the slab. Accuracy may be retained by tracking boundaries between mesh points utilising a fictitious mesh point outside of the slab and assuming a locally parabolic temperature profile. Two variants of this approach have been tested: (a) the grid moves with the velocity of the melt front, so that mesh points are removed from the back of the slab as the slab melts, and (b) a fixed spatial grid is used, so the back of the slab always lies at a mesh point, but the melt front usually lies between mesh points.

Details will only be given of method (b); for method(a) the Crank-Nicolson scheme has to be amended to include a velocity dependent term, and the treatment of the back boundary term is in the same spirit as that of the melting front in method (b). For this description it is assumed that the melt is removed, and only one phase is treated; modules may be combined for multiphase problems. Method (b) proceeds as follows:

At time t^N the distance of the melt front from the first mesh point in the slab (y_J) is $\gamma\Delta y$ (see fig 1) and the temperatures at all interior mesh points are known. The temperature T^N_{J-1} at the fictitious mesh point y_{J-1} is calculated assuming a parabolic profile through $(y_J-\gamma\Delta y, T_m)$, (y_J, T_J) and (y_{J+1}, T_{J+1}); discretization of the Stefan condition

$$\rho L u = \Phi + k(\partial T/\partial y) \qquad (2.1)$$

at the melting front gives the velocity u^N at t^N - that at t^{N+1} is predicted using u^{N-1} and u^N, so the values of γ^{N+1} may be predicted, To close the set of equations in the Crank-Nicolson formulation the back boundary condition is discretized, and T_{J-1}^{N+1} is related to T_J^{N+1} and T_{J+1}^{N+1} using the predicted value of γ^{N+1} and the assumption of a parabolic profile (ie second order accurate spatial discretization):-

$$T_{J-1}^{N+1} = (2T_m - 2(1-\gamma^2)T_J^{N+1} + (\gamma-\gamma^2)T_{J+1}^{N+1})(\gamma+\gamma^2)^{-1} \qquad (2.2)$$

The discretized diffusion equation for the slab may then be solved and the value of u^{N+1} calculated; γ^{N+1} is recalculated. Either the timestep is limited by demanding that differences between predicted and calculated velocities lead to negligible differences in front propagation (usually giving timesteps greatly in excess of that for explicit schemes) or an iterative procedure is necessary until γ^{N+1} has converged to sufficient accuracy. The calculation may be continued until only two mesh points remain in the slab. In practice to maintain a steady dependence of velocity on time, γ should not be close to zero and so the range $1.2 \geq \gamma \geq 0.2$ was chosen in preference to $1 \geq \gamma \geq 0$. This sort of modification is unnecessary for method (a) and is an advantage of that scheme.

Specimen results are shown in fig. 2. In these examples, source and sink temperatures and heat transfer coefficients are taken as constants; in accident simulations they will change with time. The first example illustrates the partial melting of a tray type catcher or reactor structure when the applied heat flux density is large (1MW m^{-2} when melting occurs) and cooling of the underneath is inefficient; an equilibrium is reached after 6 minutes when two thirds of the slab has molten. The second example illustrates melt-through of the reactor vessel, when cooling of the outside is very poor. Here with an applied heat flux density of 0.5 MW m^{-2} melt-through is completed in 200 seconds. In a series of test calculations it was found that both methods (a) and (b) gave results accurate to better than 1% using ten mesh intervals when compared with runs using more mesh points and external checks; usually method (a) (moving mesh) requires slightly fewer timesteps. Run-time for a typical problem is between one and ten seconds on the ICL 4-70. It is intended to include these algorithms in more complex simulations of melt-through phenomena.

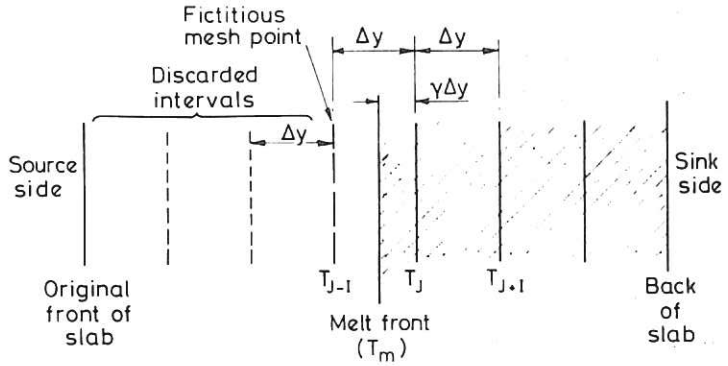

Fig.1. Mesh for one-dimensional (plane) melt-front code with fixed spatial mesh.

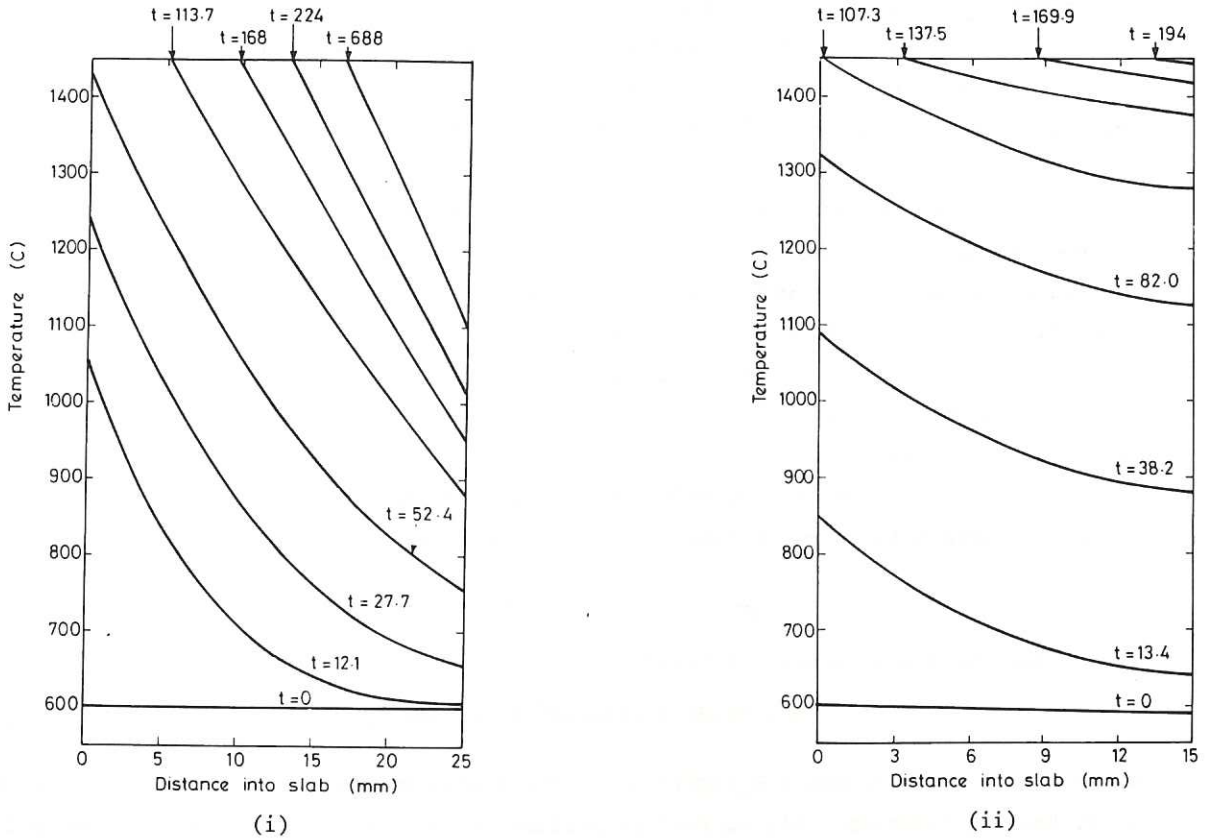

Fig. 2. Calculated temperature profiles and melting for stainless steel slabs (T_m = 1450 C) : *Case(i)* l = 0.025 m, T_{so} = 3450 C, h_{so} = 500 W m^{-2} K^{-1}, T_{si} = 600 C and h_{si} = 2000 W m^{-2} K^{-1}; *Case(ii)* l = 0.015m, T_{so} = 3450 C, h_{so} = 250 W m^{-2} K^{-1}, T_{si} = 400 C and h_{si} = 100 W m^{-2} K^{-1}. *Initially 20 mesh points were used and the average timestep was 1.3 s (unit of t is 1 second).*

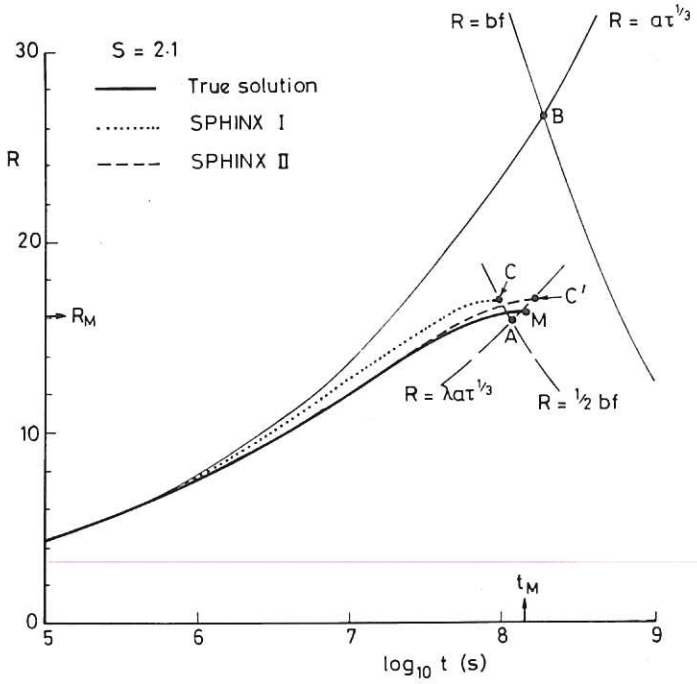

Fig. 3. The growth of the radius R of a hemispherical melt-pool as a function of time t for Stefan number S = 2.1. The true (ISOTHM) solution is represented by a heavy line ▬▬, the solution calculated by SPHINX I by..... and that by SPHINX II by – – – – –; the corresponding maximum pool sizes occur at M, C and C' respectively. The bounding curves (3.3) and (3.4) are given by thin solid curves ———, and their intersection is point B. The estimate of maximum pool size (eq. 3.7 and 3.9) is given by the point A.

3. SPHERICAL GEOMETRY : APPROXIMATE METHODS

Should the debris melt through the reactor vessel, it will proceed to melt into the concrete basemat or into a specially chosen sacrificial material. The remaining sections are concerned with the modelling of the growth of this melt-pool. A useful estimate of the pool volume can be obtained by assuming the pool grows radially using a mean heat transfer coefficient from the turbulently convecting molten pool [1]. After the initial transient, the pool temperature decays to being close to the melting point of the sacrificial bed material, and the rate at which heat is delivered to the melting front differs insignificantly from the rate of decay heat generation.

Results for pool growth based on the 1-D ISOTHM code which uses this model were given in [1]; here we develop approximations to these results which do not require the solution of partial differential equations.

The locally 1-D Fourier equation in co-ordinates moving with the melting front ($x = r - R$ where $R(t)$ is the radius of the melt pool) is

$$\frac{\partial \theta}{\partial t} = (u + \frac{2\kappa}{r}) \frac{\partial \theta}{\partial x} + \kappa \frac{\partial^2 \theta}{\partial x^2} \qquad (3.1)$$

where from the Stefan condition (2.1)

$$u = dR/dt = \kappa S(bf/R^2 + [\partial\theta/\partial x]_{x=o}) \qquad (3.2)$$

where b is a scale length ($\equiv Q_o/2\pi kT^*$), S is the Stefan number ($\equiv cT^*/L$) and f(t) is the decay heating function. All thermal properties in this section are those of the bed material, and $T^* = T_m - T_a$. Q_o is the fraction of the thermal power on stream corresponding to the amount of core debris within the pool; thus $Q(t) = Q_o f$ is the (dimensional) rate of decay heat generation within the pool (in Watts).

A simple bound for the maximum radius

Since while the melting front is advancing, the heat generated Q(t) must exceed the minimum quantity of heat which will be conducted away from a stationary pool of radius R, viz $2\pi kT^*R$, then an upper bound for the position of the advancing front is

$$R(t) = bf \qquad (3.3)$$

conversely if all the heat generated up to any instant has been incorporated into the pool then

$$R(t) = a\tau^{1/3} \qquad (3.4)$$

this provides a second upper bound. Here τ is the number of equivalent reactor seconds $\equiv \int f(t)dt$ and a is given by $a^3 = 3Q_o/(2\pi\rho[L+cT^*])$ where ρ is the density of the sacrificial bed material.

The intersection of these two curves provides a simple over-estimate R_B to the maximum radius of the pool R_M. The corresponding time t_B satisfies the implicit equation

$$\tau(t_B) = (bf(t_B)/a)^3 \qquad (3.5)$$

Fig. 3 shows point B and the two bounding curves (3.3), (3.4) when S=2, a value appropriate for many bed materials, and the decay heat function f has the form [4]

$$f = 0.11(t^{-1/4} - (t+t_q)^{-1/4}) \qquad (3.6)$$

where t_q is the irradiation time. The correct solution obtained using the 1D ISOTHM code [1] is also shown. Point B over-estimates the maximum radius by $\sim$ 60% and the time of pool maximum by $\sim$ 25% for $S \approx 2$.

Better estimates

It is clear that the maximum pool radius R_M will satisfy the simultaneous equations

$$\left.\begin{aligned} R_M &= \lambda a \tau_M^{1/\beta} \\ R_M &= \mu b f_M \end{aligned}\right\} \qquad (3.7)$$

where $\tau_M = \tau(t_M)$ and $f_M = f(t_M)$ and λ and μ lie between 0 and 1.

The heat balance equation can be written as

$$R^3(1 + G) = a^3\tau \qquad (3.8)$$

where G(t) is the ratio of enthalpy in the bed to that in the pool. Then $\lambda=(1+G_M)^{-1/\beta}$ where $G_M=G(t_M)$ and $\mu^{-1}=(-R[\partial\theta/\partial x]_{x=o})$ when $t=t_M$. Thus λ depends on an integral property whereas μ depends on a local property at the melt front.

These properties can be calculated if the temperature profile in the bed at pool maximum is known. We consider approximations based on three different assumptions:-

I. The exponential profile $\theta = \exp(-x/\delta)$ holds *throughout* the bed at the instant of pool maximum. Comparison with temperature profiles obtained using ISOTHM shows that this is a very realistic profile. This gives $R=2\delta=\frac{1}{2}bf$; correspondingly $G_M=3.75S/(1+S)$. Thus $\mu = \frac{1}{2}$ and $\lambda^3=(1+S)/(1+19S/4)$. (3.9)

With these values for λ and μ (3.7) can be solved simultaneously - a simple matter since f and τ are here assumed to have explicit algebraic forms. The resulting estimates R_A and t_A for pool maximum and time of pool maximum correspond to the point A shown on fig 3 - for $S\approx 2$.

II. The exponential profile $\theta = \exp(-x/\delta(t))$ holds in the vicinity of the melting front *at all times* up to pool maximum. Substitution into (3.1) in the vicinity of the melting front gives

$$\frac{1}{\delta} = \frac{u}{\kappa} + \frac{2}{R}$$

which enables the Stefan condition to become

$$u = \frac{\kappa S}{1+S}\left(\frac{bf}{R^2} - \frac{2}{R}\right) \qquad (3.10)$$

This is an ordinary differential equation for the position of the melting front which can be integrated using a standard ODE solver. This has been implemented in SPHINX I, and leads to R_C and t_C as estimates for pool maximum and time of pool maximum, corresponding to the point C shown on fig 3 for $S\approx 2$.

III. The exp - erfc profile $\theta = (R/r)\exp(-ux/\kappa)\operatorname{erfc}(x/(2\sqrt{\kappa t}))$ holds in the vicinity of the melting front *at all times* to pool maximum. This hybrid form tends to the 'fast melting front solution' when $x \ll \sqrt{\kappa t}$ and to the external solution for a sphere of radius R when $u \to 0$. Substitution in (3.2) for $(\partial\theta/\partial x)$ at the melting front gives

$$u = \frac{\kappa S}{1+S}\left(\frac{bf}{R^2} - \frac{1}{R} - \frac{1}{\sqrt{\pi\kappa t}}\right)$$

(cf 3.10) The solution of this ODE here called SPHINX II, leads to $R_{C'}$ and $t_{C'}$ at pool maximum corresponding to the point C shown in fig 3.

Table 1 shows a comparison of these estimates of the pool maximum and corresponding time for a wide range of values of the Stefan number for long irradiation times.

S	True Solution M		Estimate A		Estimate B		Estimate C		Estimate C'	
	R_M(m)	t_M(s)	R_A/R_M	t_A/t_M	R_B/R_M	t_B/t_M	R_c/R_M	t_c/t_M	$R_{c'}/R_M$	$t_{c'}/t_M$
0.04	10.67	8.34×10^8	1.03	0.35	1.32	0.93	0.88	0.50	1.02	1.13
2.1	16.10	1.45×10^8	0.99	0.80	1.66	1.26	1.05	0.66	1.04	1.16
105	16.55	1.07×10^8	0.98	1.03	1.75	1.38	1.10	0.73	1.05	1.22

Table 1. Maximum Pool size R_M and associated time t_M, with the estimates corresponding to point A, B, C, and C' (see fig.3).

From this the following conclusions may be drawn:

(i) The maximum radius for a hemispherical cavity produced by decay heating can be approximated to within 3% by the algebraic formulae (3.7) and (3.9) over the whole range of Stefan numbers. The time of pool maximum can be estimated to much better than 50% by the use of (3.5). These formulae give this accuracy with 10 to 20 evaluations of the function τ/f^3 which is assumed known, at least in tabular form.

(ii) Use of the exp-erfc profile (approximation III) leads to a single ODE for the position of the advancing front, which follows the growth of the cacity for several years, and results in maximum pool sizes accurate to 5% for all values of S and times of pool maximum over-estimated by less than 25%. It is much cheaper than solving (3.1) with (3.2) as a partial differential equation by any of the available methods, but of course the accuracy achievable is limited.

The generalization to non-spherical geometries of these approximate methods for tracking the position of the melting front is discussed in [4].

4. SENSITIVITY STUDIES USING PAMPUR

The approximations discussed above and the ISOTHM results give conservative estimates for the pool volume. More realistic models must allow for the variation in aspect ratio of the pool as it develops. The PAMPUR 3 code [1] for the growth of axisymmetric pools into an underlying solid does allow the aspect ratio to evolve, with the assumption that the pool may be considered as a single phase in which natural convection is driven by internal heating. Good heat transfer to the overlying sodium is assumed and heat transfer coefficients are based on the studies of Kulacki and co-workers [5,6]. It is assumed that the pool may be approximated by a hemispheroid. Conduction into the bed is modelled using one-dimensional forms of the isotherm migration method along the vertical axis and the pool periphery ; the curvature of the isotherms is usually calculated from the shape assumption. Because of the high aspect ratios found with the current heat transfer model a hemispheroid is probably not the best choice for the pool shape, but the results should reflect the behaviour of more realistically shaped pools.

A parametric study has been carried out for the debris from a 3.2 GWt reactor melting into a basalt bed, using the data given in [1]. The effect on pool volume of assuming different values for the conductivity of the bed (usually taken as 2 W $m^{-1}K^{-1}$) is shown in Fig 4 ; at later times significant reduction in pool volume results with increased thermal

conductivity. For values of k between 0 and 10 W m^{-1} K^{-1} the aspect ratio (radius/depth) is in the range 7.5 - 9.5 at times between one and twenty days after melt-through.

The assumed viscosity of the molten bed (usually taken as $\nu = 10^{-6} m^2 s^{-1}$) was also varied over a wide range ; the dependence of pool temperature on assumed viscosity for various times after melt down is shown in Fig 5. At early times low viscosity pools cool rapidly whilst high viscosity pools boil ; for realistic values of viscosity pool boiling will cease within two hours of pool formation. Changing the assumed viscosity has some effect on pool volume ; after 11 days the predicted volume is $348m^3$ (depth 1.44m, radius 10.7m) for $\nu=10^{-5} m^2 s^{-1}$ compared with $267m^3$ (depth 1.14m, radius 10.5m) for $\nu = 10^{-6} m^2 s^{-1}$. Because viscosity enters the calculation through the Rayleigh number, it only occurs in the combination (β/ν) where β is the thermal expansion coefficient of the liquid, so the results may be used to consider a range of values for β for fixed viscosity.

Much smaller pools result if magnesia is chosen as the sacrificial material in preference to basalt; for instance after 4 days the predicted pool volume is $23m^3$ compared with $165m^3$ for basalt, but the pool temperature is necessarily much higher for a magnesia bed as the melting point of the bed is greater, and pool boiling may occur for considerably longer. (Eutectic formation, ignored in the calculations for magnesia, may lead to somewhat larger pools but reduced temperatures).

In general the maximum pool radius expected from the PAMPUR calculations is similar (perhaps 10-20% smaller) than that for the equivalent ISOTHM calculation (see [1]) or hemispherical approximation (see above), but the depth of the pool is much reduced ; a more realistic heat transfer model, including disruption of the stable lower layer

Fig. 4. Parametric study for melt-down of 3.2 GWt reactor core onto a basalt bed using the PAMPUR code - dependence of pool volume (including crust) on bed thermal conductivity at various times after melt-down.

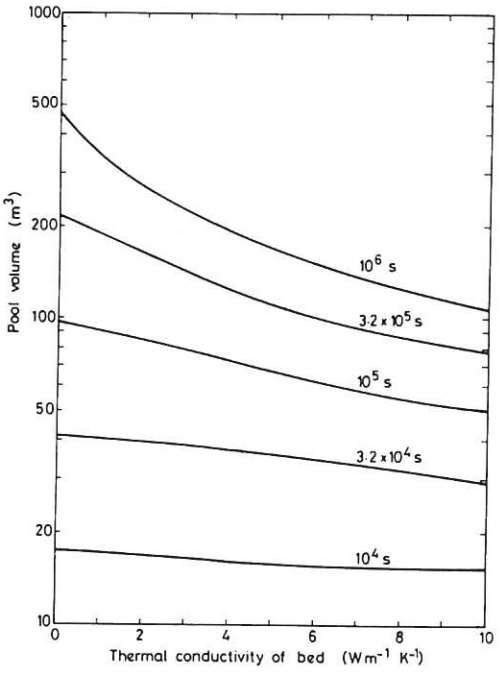

Fig. 5. Dependence of maximum pool temperature on assumed kinematic viscosity at various times after melt-down. (Initial depth = 0.30 m.) The temperatures for the pool boiling regime (shown dotted) are over-estimates.

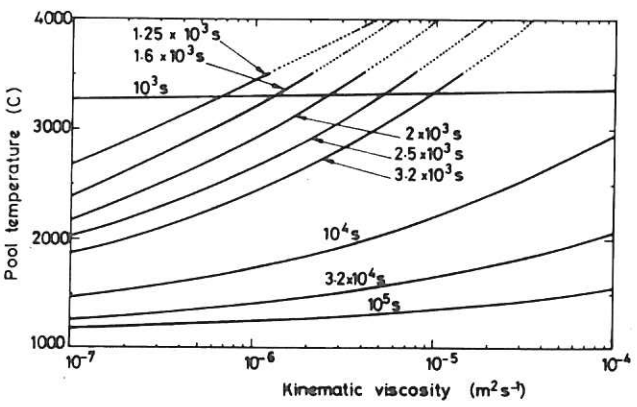

in the pool, would lead to greater depths and somewhat reduced radii besides reducing the likelihood of pool boiling.

In a later version of the code, heat removal by the sodium is considered in more detail together with crust formation at the pool surface. For the standard run (initial debris depth 0.30m) sodium boiling at the pool surface is expected until 4 hours after melt-down, but the critical heat flux is not exceeded. Assuming a heat capacity of the sodium and reactor internals equal to 1.1×10^{10} J K^{-1}[7], an initial (rather high) sodium temperature of 600°C, and a sink temperature of 100°C the peak sodium temperature is 667°C (after 2 days) if the heat transfer coefficient is 10kW K^{-1}. Changing the assumed heat transfer coefficient hardly effects the pool growth (unless sodium boils off) - as the sodium temperature remains higher for longer with a low heat transfer coefficient a thinner crust on the pool results (e.g. at 11 days the crust thickness is 73mm for cooling of 20kW K^{-1} but only 34mm for cooling of 10kW K^{-1}).

5. MULTIDIMENSIONAL FORMULATION OF THE ISOTHERM MIGRATION METHOD

The PAMPUR 3 code is mainly of use in the early and medium timescales (up to a few x 10^6s) ; if pool growth is unconstrained by cooling systems or highly refractory barriers, accurate modelling to determine the maximum pool dimensions requires the solution of a multidimensional Stefan problem. As in the PAMPUR codes the calculations may be split into two parts

(i) conduction into the bed and melting of fresh bed material and

(ii) a model for heat and mass transfer within the pool.

The input for (i) is a position dependent heat flux density calculated using (ii). The heat transfer model of (ii) besides being dependent on the pool shape determined in (i) may also depend on the rate of melting calculated in (i). We concentrate here on part (i) ; work on part (ii) is still at a preliminary stage.

With the formulation outlined above, a front-tracking method is preferable to an enthalpy (weak) method, particularly if heat transfer is to be related to melting rate. Few tested methods are available for this type of problem ; notable progress has been made by Laziridis [8] where the added geometrical complications of going to higher dimensions are obvious and by Meyer [9] both of whom use fixed spatial meshes. In growth of melt-pool studies the spatial region of interest changes as the pool grows and the thermal front broadens. It is likely that if a fixed spatial mesh is used, in order to keep the coding simple, much of the calculation would be at mesh points where the temperature is only changing slowly, leading to inefficiency. It was noted that for one dimensional problems the isotherm migration method (IMM) does not suffer this drawback and also gives a simple treatment of the melt-front. In a more detailed study of the IMM [10] a conservative formulation for one-dimensional problems has been developed which reduces significantly the number of isotherms required for accurate computation. A generalization for multidimensional problems has been developed which is appropriate for a melt pool code.

We consider first the one dimensional spherically symmetric problem, originally solved in ISOTHM. The IMM equation, which is obtained by a co-ordinate transformation of the Fourier equation, can be written in the form

$$\frac{\partial \Psi}{\partial t} + \frac{\partial \Omega}{\partial T} = 0 \qquad (5.1)$$

where $\psi = \rho c r^3/3$ and $\Omega = k r^2 /(\partial r/\partial T)$ for $r = r(T,t)$; c and k may be temperature dependent. Discretization of (5.1) on a uniformly spaced temperature mesh leads to a conservative scheme (see e.g. [11]) for the quantity

$$I(t) = \int_{T_a}^{T_m} \Psi \, d\, T \qquad (5.2)$$

provided the endpoints are treated correctly (see [10]). The Stefan condition (2.1) may be written as

$$\frac{L}{C}\frac{\partial \Psi}{\partial t} = R^2 \Phi - \Omega\Big|_{T=T_m} \qquad (5.3)$$

and it can be shown that for the melt-pool application

$$I(t) = I(t_o) + \int_{t_o}^{t} \frac{Q(t')dt'}{2\pi} - \left[\frac{\rho L R^3}{3} \right]_{t_o}^{t} \qquad (5.4)$$

where t_o is the start of the calculation. This heat balance is necessarily satisfied by the discretized form.

A revised version of the ISOTHM code used for results in [1], which incorporates this conservative form of the IMM, needs as few as six isotherms for better than 1% accuracy.

Multidimensional versions of the IMM have been used by Crank and co-workers [12,13] and Durack and Wendroff [14]. Unlike those versions that proposed here uses a complete co-ordinate transformation ; one spatial co-ordinate is chosen as the new dependent variable and the independent variables are the remaining spatial co-ordinates and temperature. For fixed values of the other independent variables the dependent variable should be a monotonic function of temperature.

In [10] general equations of the form

$$\frac{\partial \psi}{\partial t} = -\left(\frac{\partial \Omega^T}{\partial T} + \frac{\partial \Omega^\beta}{\partial \beta} + \frac{\partial \Omega^\gamma}{\partial \gamma}\right) \qquad (5.5)$$

are derived based on orthogonal curvilinear co-ordinate systems (α,β,γ) where α is the new dependent variable. For spherical polars (Γ,θ,ϕ), $\Gamma \equiv \alpha$, $\theta \equiv \beta$ and $\phi \equiv \gamma$. For axisymmetric configurations with $(\partial/\partial\phi) \equiv 0$, we find that

$$\Psi = \rho c r^3 \sin\theta/3$$

$$\Omega^T = k \sin\theta (r^2 + (\partial r/\partial\theta)^2)\ (\partial r/\partial T)^{-1}$$

$$\Omega^\theta = -k \sin\theta (\partial r/\partial\theta)$$

The condition at the melt-front is

$$\frac{L}{C}\frac{\partial \psi}{\partial t} = \left(r^2 + \left(\frac{\partial r}{\partial \theta}\right)^2\right)^{\frac{1}{2}} \Phi \sin\theta - \Omega^T\Big|_{T=T_m} \qquad (5.6)$$

these relations may be used to construct a conservative scheme analogous to that used for one-dimensional problems. The calculational mesh (see fig 6.) is uniformly spaced in temperature and angle, and a nodal volume is associated with each mesh point. The flux terms of the LHS of (5.5) are evaluated at the boundaries between adjacent volumes.

A specimen calculation for the growth of a melt pool in a basalt bed is show in fig. 7. It is assumed that two thirds of the decay heat is taken upwards and Q_o = 3.2 GWt. The applied heat flux function is such as would maintain a hemispheroidal pool with an axial ratio of four were conduction into the bed negligible.

There is thus the capability of solving accurately and efficiently for heat conduction into the bed and the associated melt pool growth, if the heat flux function is known. To benefit from this it is necessary to develop reliable heat transfer models for arbitrarily shaped pools from the various experimental and theoretical investigations.

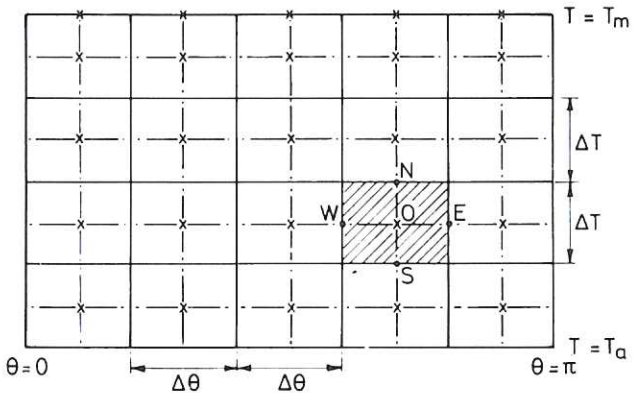

Fig.6. Mesh in (θ,T) space for multi-dimensional IMM. Mesh points are indicated by crosses. A typical cell is shown hatched. In the calculation Ω^T is evaluated at points N and S to construct $\partial\Omega^T/\partial T$ and Ω^θ is evaluated at points E and W to construct $\partial\Omega^\theta/\partial\theta$. Ψ is evaluated at the mesh point O.

Fig 7. Example of multi-dimensional IMM calculation. The pool is shown hatched, and the melt-front (solid), the $0.5\ (T_m + T_a)$ *isotherm (long dashes) and the* $[0.1\ T_m + 0.9\ T_a]$ *isotherm (short dashes) are shown for various times after pool formation. The calculation was started at* $t = 3 \times 10^5$s.

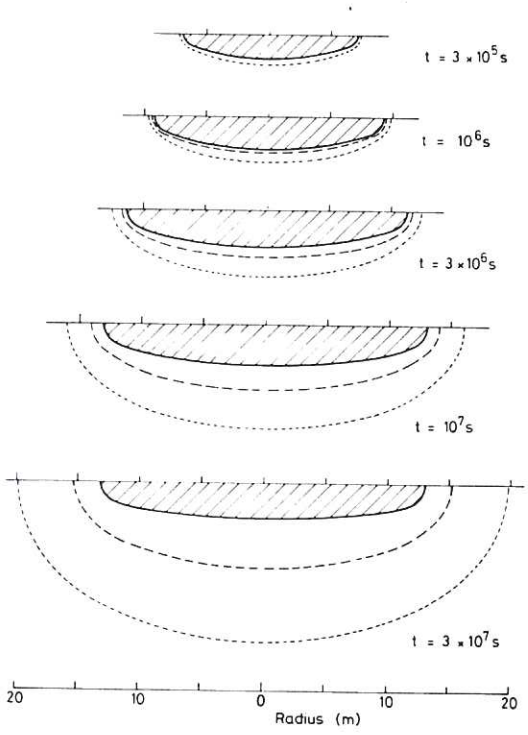

6. DISCUSSION

The understanding of melting front behaviour is best achieved by considering the results from a number of different simplified models rather than putting all the possible effects, many of which are rather uncertain into one model. For broad shallow pools, the depth of penetration can be adequately calculated using plane slab models. For deeper pools of smaller aspect ratio, hemispherical models provide useful estimates of maximum pool volume and extent. Hemispheroidal models such as PAMPUR enable the dependence of aspect ratio of the pool on thermophysical properties to be examined relatively cheaply. For detailed calculations, and for cross-checks on the validity of the simplified models, a full multidimensional model is required, and the generalized form of the IMM is well suited to this.

The circumstances under which the PAMPUR code is applicable are discussed in §4 of [1]. The multidimensional IMM and the generalization of the approximate methods described in §3 only couple to the detail of the behaviour within the pool via heat transfer coefficients at the melting front and so the methodology is independent of the assumption of a well mixed pool which underlies this approach ; thus multiphase pools with gas agitation can be handled by incorporating additional computational modules.

The structure and stability of the upper surface of a molten pool is an important area which merits further examination. The melt front is assumed to be a smooth curved surface in this paper. The possibility of ripples and 'fingering' at the melt surface was discussed in [16]; the effects of cracks in the bed material are examined in [15].

NOMENCLATURE

a	$3Q_o/(2\pi\rho(L + c\,T^*)$
b	$Q_o/2\pi kT^*$ (Scale length)
c	specific heat
$f(t)$	decay heat function
G	enthalpy of bed/enthalpy of pool
h	heat transfer coefficient
k	thermal conductivity
I	defined in §5
ℓ	thickness of slab
L	latent heat of fusion
Q_o	full thermal power of debris in reactor
$Q(t)$	decay heating rate ($=Q_o f(t)$)
r	radial co-ordinate
R	pool radius
S	Stefan number($=cT^*/L$)
T	temperature
T^*	$T_m - T_a$
u	velocity of melt front
x	spatial co-ordinate moving with melt front
y	stationary Cartesian co-ordinate
(α,β,γ)	general curvilinear co-ordinates
β	thermal expansion coefficient of liquid
γ	(displacement of melt front from mesh point)$/\Delta y$
δ	scale length of thermal front
Δ	mesh spacing (prefix)
Θ	dimensionless temperature
Θ,ϕ	polar angle co-ordinates
κ	thermal diffusivity ($k/\rho c$)
λ	$(1 + G_M)^{-1/3}$
ν	kinematic viscosity
ρ	density
τ	$\int_o^t f(t)dt$
Φ	heat flux density from liquid
Ψ	defined in §5
Ω	defined in §5

SUBSCRIPTS

a	ambient
A,B,C,C'	refer to different approximations discussed in §3
J,J+1	mesh numbers
m	melting;melt front value
M	maximum (of pool)
o	initial value
si	sink
so	source

SUPERSCRIPT

N	timestep number

ACKNOWLEDGMENTS

P. S. Jackson, M. J. Bleach and G. Wilson assisted with numerical computations. This work has been supported by the UK Safety and Reliability Directorate, Culcheth.

REFERENCES

[1] R S Peckover, B D Turland and R T P Whipple : On the growth of melting pools in sacrificial materials, in *"Proc. 3rd. P.A.H.R. Information Exchange"* (ANL-78-10) (1978)

[2] L Fox : What are the best numerical methods (for Stefan problems)? in *"Moving Boundary Problems in Heat Flow and Diffusion"* (p210), J R Ockenden and W R Hodgkins (eds) Oxford (1975)

[3] J Crank and P Nicolson : A practical method for numerical integration of solutions of partial differential equations of heat conductive type. Proc. Camb. Philos. Soc. 43 , 50 (1947)

[4] R S Peckover : Thermal moving boundary problems arising in reactor safety studies. Paper presented at Durham symposium on free and moving boundary problems in heat flow and diffusion. Culham Preprint CLM-P562 (1978)

[5] F A Kulacki and A A Emara : Steady and transient thermal convection in a fluid layer with uniform volumetric energy sources. J. Fluid Mech 83 375 (1977)

[6] L Baker Jr, R E Faw and F A Kulacki : Post Accident Heat Removal II ; Heat transfer within an internally heated, non-boiling liquid layer. Nuc. Sci. and Eng. 61, 222 (1976).

[7] D Broadley and R N McSweeney : Sizing of decay rejection loops for LMFBRs. in *"Optimisation of sodium cooled fast reactors"* (p117). B.N.E.S. (1978).

[8] A Laziridis : A numerical solution of the multidimensional solidification or melting problem. Int. J. Heat Mass Transfer 13, 1459 (1970).

[9] G H Meyer : Numerical Methods. Paper presented at Durham symposium on free and moving boundary problems in heat flow and diffusion (1978).

[10] B D Turland : Conservative Isotherm Migration Methods for Stefan problems (in preparation) (1978).

[11] D Potter : Computational Physics (p63) John Wiley & Sons (1973).

[12] J Crank and R S Gupta : Isotherm migration method in two dimensions, Int. J. Heat Mass Transfer 18, 1101 (1975).

[13] J Crank and A B Crowley : Isotherm migration along orthogonal flow lines in two dimensions. Int. J. Heat Mass Transfer 21, 393 (1978)

[14] D Durack and B Wendroff : Computing a two-dimensional quench front. Nucl. Sci. and Eng. 64, 187 (1977).

[15] R S Peckover, J H Adlam and B D Turland : On the effects of cracks within sacrificial bed material on the growth of molten pools. 4th PAHR information exchange. Ispra (1978).

[16] B D Turland, R S Peckover and T A Dullforce : On the stability of advancing melting fronts to spatial perturbations in *"Proc. 3rd P.A.H.R. Information Exchange"* (ANL-78-10) (1978).